Article

Not peer-reviewed version

# DNA Gene's Basic Structure as a Nonperturbative Circuit Quantum Electrodynamics: Is RNA Polymerase II the Quantum Bus of Transcription?

ANNIE RIERA LEAL *, RAUL RIERA AROCHE, YVETH MARLENE ORTIZ GARCIA, ESLI CAMILA SANCHEZ MORENO, JOSE SAULO ENRIQUEZ CERVANTES, ANDREA CAROLINA MACHADO SULBARAN

Posted Date: 25 September 2024

doi: 10.20944/preprints202409.1016.v2

Keywords: DNA gene's basic structure; circuit quantum electrodynamics; quantum bus of transcription

*Article*

# DNA Gene's Basic Structure as a Nonperturbative Circuit Quantum Electrodynamics: Is RNA Polymerase II the Quantum Bus of Transcription?

**Raul Riera Aroche [1,2], Yveth M. Ortiz García [2,3], Esli C. Sánchez Moreno [2,4], José S. Enriquez Cervantes [2,4], Andrea C. Machado Sulbaran [2,5] and Annie Riera Leal [2,4,*]**

[1] Department of Research in Physics, Division of Natural Sciences and Mathematics, University of Sonora, Hermosillo, Sonora, México.
[2] Research and Higher Education Center of UNEPROP, Hermosillo, Sonora, México.
[3] Institute of Research in Dentistry, Department of Integral Dental Clinics, University Center of Health Sciences, University of Guadalajara, Guadalajara, Mexico.
[4] Department of Dermatology, General Hospital of the State of Sonora, Hermosillo, Sonora, México.
[5] Childhood and Adolescence Cancer Research Institute, University Center of Health Sciences, University of Guadalajara, Guadalajara, Mexico.
* Correspondence: annierieraleal78@yahoo.es
Annie Riera Leal, PhD, Address: Boulevar José María Escrivá de Balaguer 157. Colonia Villas del Palmar, C.P. 83105. Hermosillo, Sonora. México; Phone: (00 52) 6623497429; E-mail: annierieraleal78@yahoo.es; ORCID: 0000-0002-6499-656X

**Abstract:** Previously, we described that Adenine, Thymine, Cytosine, and Guanine nucleobases were superconductors in a quantum superposition of phases on each side of the central Hydrogen bond acting as a Josephson Junction. Genomic DNA has two strands wrapped helically around one another, but during transcription, they are separated by the RNA polymerase II to form a molecular condensate called the transcription bubble. Successive steps involve the bubble translocation along the gene body. This work discusses how quantum information transfer and entanglement can be achieved by modeling DNA as a combination of $n$ nonperturbative circuits quantum electrodynamics with nine Radio-Frequency-Superconducting Quantum Interference Devices (SQUIDs) inside. A bus can be coupled capacitively to a single-mode microwave resonator. The cavity mode and the bus can mediate long-range, fast interaction between neighboring and distant DNA SQUID qubits. RNA polymerase II produces decoherence during transcription. This enzyme is a multifunctional biomolecular machine working like an artificially engineered device. Phosphorylation reactions catalyzed by protein kinases constitute the driving force. The coupling between $n$ phosphorylation pulses and any particular SQUID qubit can be obtained selectively via frequency matching.

Keywords: DNA gene's basic structure; circuit quantum electrodynamics; quantum bus of transcription

## 1. Introduction

Structure-function transcription studies revealed a highly evolutionary conserved process for all three life divisions. Transcription is divided into three steps: promoter DNA binding and RNA initiation, processive RNA chain elongation, and termination [1]. Key points of each step were elucidated, including the nucleotide (nt) addition cycle, and the RNA proofreading mechanism after recognizing errors [2]. Also, a similar architecture, active center, and transcription mechanism of cellular RNA polymerases (RNA pol) have been described [3]. Using nucleoside triphosphate (NTP) substrates, RNA pol synthesizes the RNA complementary to the DNA template strand. The transcription process occurs spatially, forming biomolecular condensates, and RNA pol II can be incorporated into them [2,4].

 doi:10.20944/preprints202409.1016.v2



The qubit, the elementary block for quantum information processing [5], is equivalent to a two-level quantum system (TLS) [6]. Some systems have naturally qubit properties, such as nuclear, atomic, molecular spins, electric dipoles [7], and DNA base pairs (bp). Previously, we carried out a theoretical approach to DNA as a quantum computer [8]. In DNA qubits, Adenine (A) and Thymine (T), Cytosine (C), and Guanine (G) are paired superconductors with the central Hydrogen bonds (H-bond) acting as a Josephson Junction (JJ). The quantum tunneling of H in DNA and RNA has been described [9]. Qubits have to store information, be able to be manipulated, and the data must be transferred effectively (quantum bus). Maintaining the quantum coherence of qubits is a critical challenge. The system must be insensitive to external disturbances [10].

The central idea for multiple qubit architectures is based on coupling them to a transmission line and selecting from the frequency at which qubits couple together [11,12]. These behave as non-linear resonators in which the fundamental and excited levels can be isolated. The general scheme of a coplanar microwave transmission line consists of a one-dimensional cable evaporated on an insulating substrate with two superconducting planes parallel to it on the same surface [13,14]. A finite transmission line is obtained by interrupting the central wire at two points to get a resonator that supports a quantized electromagnetic mode, behaving as a harmonic [15].

Cavity Quantum Electrodynamics (cavity QED) studies an atom as a TLS and the quantized electromagnetic field within an optical cavity [16]. Inspired by the circuit QED, Circuit Quantum Electrodynamics (circuit QED) emerges, in which superconducting qubits and microwave transmission lines called resonators replace the atoms and the cavity, respectively [13,17]. A TLS and a coupled harmonic oscillator exist in the cavity QED and the circuit QED [16–18].

Superconducting resonators are crucial elements in a circuit QED [17]. A microwave resonator can be an excellent quantum bus for qubit manipulation and memory [11]. In the cavity QED, the atom couples to the electromagnetic field through its electric dipole moment, while superconducting qubits have several coupling alternatives [19]. Circuit QED is a well-suited platform for quantum data due to its flexibility, scalability, and tunability [20]. Experimental works demonstrated superconducting qubits and a microwave resonator strong coupling [21].

Developing a molecular circuit engineering that controls the haphazard states of individual molecular events is a big challenge. In this work, an electrical representation of DNA is carried out following the Quantum Electrodynamics Theory of Circuits and considering the results previously published by our team [8]. A gene is described as a problem of a qubit capacitively coupled to two transmission guides subject to a harmonic forcing in the magnetic flux that passes through it for a frequency $\omega_r$ and an amplitude $A$. A-T, T-A, C-G, and G-C bp are structurally similar to Radio Frequency Superconducting Quantum Interference Device (RF-SQUID), where each level is coupled to a different transmission line. In a resonant regime, the separation between the two energy levels of the qubit is in resonance with the frequency of the transmission lines. Entangled qubit-photon states are generated, and both system parts could exchange excitations. We consider genes as a combination of $n$ single-mode microwave resonators and cavities coupling in parallel. The Frequency matching can selectively obtain coupling between the phosphorylation pulse emitted by RNA pol II and any particular SQUID bp during transcription.

## 2. DNA and Transcription: Structural and Biochemical Studies

Genomic DNA is double-stranded. The H-bonded bases are assembled in parallel, perpendicular to the helix backbone. The x-ray analysis revealed a regular space of 0.34 nm between the bases and 36° of twist angle about the helical axis. Ten pairs of bases define the helix anatomy of a complete turn every 3.4 nm [22,23]. A repeating sugar (deoxyribose)- phosphate units form the strand backbone [23]. Each bp triplet constitutes a codon that carries on the genetic code. However, most of the human genome does not code for proteins. These regions may provide RNA molecules and transcription factors' specific sequences of binding sites and exert regulatory functions [24]. The minor and major grooves are two helical spaces with different widths. The first one is delimited by the space when the two antiparallel DNA strands run closest together, while the major groove is

Preprints.org (www.preprints.org) | NOT PEER-REVIEWED | Posted: 25 September 2024 doi:10.20944/preprints202409.1016.v2



defined when they are furthest apart [22]. The above information is the DNA B schematic representation, the predominant type in most cell DNA stretches [23].

The eukaryotic transcription cycle arises during three phases. The RNA chain initiation undergoes various steps, recruiting multiple cellular factors, the mediator complex, and the RNA pol II to form a pre-initiation complex (PIC) at core promoter sequences. PIC composition is identical at all yeast promoters and is the rate-limiting step for transcription [25]. After, the RNAP II accesses the DNA template strand to begin the RNA synthesis. All cellular RNA pol II forms a stable elongation complex (EC) with the DNA template and RNA transcript for transcription elongation [26].

Eukaryotic polymerases comprise an evolutionarily conserved catalytically competent ten-subunit core and up to seven peripheral subunits. The C-terminal domain (CTD) of the RNA pol II largest subunit has a repeated heptad motif ($Tyr_1Ser_2Pro_3Thr_4Ser_5Pro_6Ser_7$) [27]. The copy number depends on the organism's complexity (26 in yeast vs. 52 in humans). CTD's dynamic phosphorylation (P) and dephosphorylation coordinate the specific association and release of transcriptional factors at every stage of transcription (Figure 1A) [28,29]. For example, transcription initiation and promoter escape at the 5′-end are facilitated by $Ser_5$-P for Kin28/Cdk7, while for the elongation $Ser_5$-P is by Srb10/Cdk8 and collaborates $Ser_2$-P by Ctk1/Cdk9. The termination and the 3′-end processing are because of the $Ser_2$-$Ser_2$-P transition by Bur1/Cdk9 [30,31]. A similar P-process regulates the biological activity of many proteins.

In most promoters, the two main recognition consensus sequences TTGACA and TATAAT (−35 and −10 hexameric boxes) are separated by a region of 17 ±1 bp called a spacer [32,33]. The −35 element interacts with the σ4 domain and the DNA major groove by inserting a helix-turn-helix (HTH). The −43 to −38 sequences interact with the DNA minor grove and the $\alpha$-CTD [34]. During elongation, the transcription bubble has a 12±1 nt constant size and 8±1 bp RNA–DNA hybrid until RNA pol II reaches a termination codon [35]. RNA pol II selects the correct nt, adds it to the growing RNA chain 3′-end, and releases pyrophosphate ($PP_i$). The same residues contacting the nt exist in all RNA pol, consistent with a general nt addition cycle (NAC) [36]. The NTP substrate attaches transiently to the open active center enzyme conformation. Structural information on an RNA pol II EC revealed a nine-base pair DNA-RNA hybrid duplex from the active center cleft at the floor [2,37,38].

In the transcription bubble, DNA is unwound before the RNA pol II catalytic site, allowing the template single strand to reach it and form the DNA-RNA hybrid duplex. It is then rewound to assemble the exiting DNA duplex. Within the unwound region, the growing RNA is attached to the active center cleft with its 3′-end and forms the nine bp hybrid duplex with the DNA template strand [26]. The high EC stability depends on the DNA-RNA tight binding and facilitates transcription processivity. Again, CTD-P plays an important role. $Spt_5$ spans the pol II cleft from the clamp, and contacts upstream DNA, and the non-template DNA strand [39]. $Spt_5$ positive charges interact with the negatively charged DNA non-template strand to prevent the bubble's collapse. The $Spt_5$ NGN domain links to all polymerases clamp in the coiled-coil [36], indicating an evolutionary conserved binding mode.

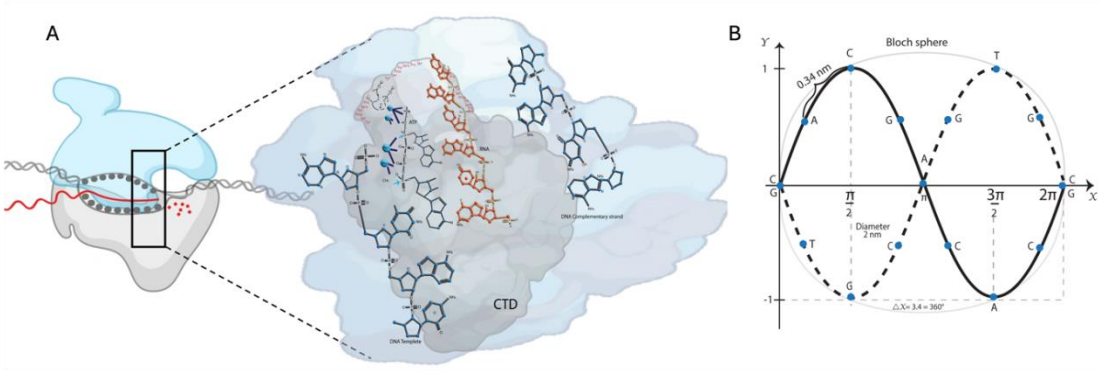


**Figure 1. Quantum model of transcription**. A) The RNA pol II sends the system pair of pulses with the same parameters ($n$) times. RNA pol II driving force is manifested by processive phosphorylation of alcohol residues in RNA pol II using ATP as the phosphate donor. It produces a rotation of the

 doi:10.20944/preprints202409.1016.v2



point on the sphere concerning the rotation axis at the rotation angle. Thus, it extracts the number of times the system was in the state $|0\rangle$ or $|1\rangle$. When the flow phase shift occurs, the Bloch sphere is reproduced. B) Representation of the DNA strands in the transition to the Bloch sphere as a symmetric and antisymmetric function: $y = A\ sin\ sin\ x$ and $y = -A\ sin\ sin\ x$ .

### 3. A-T, T-A, G-C, AND C-G Base Pairs: RF Squids—The Hamiltonian Scheme

Superconducting qubits steam as a leading technology platform for quantum computing [11,40]. Flux qubits exploit magnetic flux through a superconducting loop. A superconducting ring is interrupted by one or more JJs and crossed by a magnetic flux based on the Josephson Effect [11]. The qubit's quantum state is encoded in the persistent loop current and manipulated by altering the magnetic flux. Suppose an external oscillating flow of fixed frequency and variable amplitude is applied. In that case, the qubit can be forced by generating oscillations in the populations of its two energy levels through the Landau-Zener-Stuckelberg Transitions.

Phase qubits store quantum information in the difference of phases between the JJ on both sides. The quantum states coherent rotations can be induced by applying external microwave pulses [41]. One of the most used systems in Circuit QED is the charge qubit (Cooper pair box) coupled through the electrical component of the field to a superconducting coplanar waveguide resonator [40]. Recently, many studies have highlighted the central role of transmon qubits (Figure 2A) in quantum computing [19]. In them, the superconducting island is controlled by an external magnetic field that induces a magnetic flux across the JJs, affecting the superconducting phase difference [11,13].

An anharmonicity with a high energy difference between consecutive levels ensures well-defined qubits and long-lasting quantum calculations. In a previous study, our working group established the role of DNA as a perfect quantum computer by characterizing Adenine (A), Thymine (T), Cytosine (C), and Guanine (G) nitrogenous bases as superconducting islands. In addition, we defined DNA qubits by combining the system quantum state with classical information:

$|0\rangle[A\ T\ ] = |0\rangle[T\ A\ ] = |0\rangle[X]$, and $|1\rangle[G\ C\ ] = |1\rangle[C\ G\ ] = |1\rangle[Y]$

A-T and C-G are superconducting qubits with intrinsically quantum behavior. They have quantized energy levels, so their separation is more significant than thermal fluctuations and can be in superposition states. The JJ introduces anharmonicity to the system [11], thus obtaining non-equispaced energy levels. Each transition has a distinct frequency because of the decreasing energy spacing as the quantum number progressively increases. If externally applied a magnetic flux, the double-well potential and the two eigenfunctions become symmetrical while antisymmetrical superpositions of the two basis states. In these superconducting rings, a single total wave function describes the state of all electron and hole pairs in the condensate: $\psi_{\vec{p}} = \psi e^{i\vec{p}.\vec{r}/\hbar}$.

$\vec{p}$ single electron and hole pair momentum.

$|\psi|^2$is the probability density of finding an electron and hole pair in a given volume

$\vec{p}.\vec{r}\ /\ \hbar$ of the phase associated with each electron and hole pair in space.

Because this wave function must be unvalued, the accumulated phase change $(\Delta\emptyset)$ when traveling a closed path around the year must be a multiple of $2\pi$:

$\Delta\emptyset = 2n\pi$ where $n$ is an integer number

Because the RNA pol II contacts only one element of the pair (classical information) in the template strand, we considered the number of aromatic rings to get one of the four Bell states:

Purines $= |0\rangle$, Pyrimidines $= |1\rangle$, then

$|\psi\rangle A = |\psi\rangle G = |0\rangle$, and $|\psi\rangle T = |\psi\rangle C = |1\rangle$, then

$|0\rangle[X] = |0\rangle[01]$ or $|0\rangle[10]$, and $|1\rangle[Y] = |1\rangle[01]$ or $|1\rangle[10]$

$|\psi\rangle AT = [00]$, $|\psi\rangle TA = [01]$, $|\psi\rangle CG = [11]$, and $|\psi\rangle GC = [10]$

A JJ forms the foundation of a SQUID. However, these junctions also present an internal capacitive effect because they are constituted by two superconducting electrodes separated by an insulator [11]. The JJ can be considered a linear harmonic LC circuit with nonlinear inductance. Two types of SQUIDs are commonly used in quantum computer applications: a DC SQUID, which contains two parallel junctions, and an RF SQUID, which includes just one junction.

 doi:10.20944/preprints202409.1016.v2



In DNA qubits, the central H-bond, acting like a JJ, forms the foundation of the RF SQUIDs (Figure 2B). The H-bond can induce strong inter- or intra-molecular electronic coupling by enhancing resonance, electron delocalization, or planarizing the conjugated backbone.

Nitrogenous (N) number three (N3) of a T in T-A bp has a lone pair of electrons as part of the $\pi$-cloud. The N1 in A uses the lone pair to attract the H attached to the N3 of T. Similarly, in C-G bp, the N3 in C uses its lone pair of electrons to form an H-bond with the N1 of G. Then, in our previous work, we explained, using physics approximations, how electrons interchange a biological quantum of energy to form electrons and hole pairs in the JJ. The electron ($e$) three ($e_3$) with the momentum $P + K$ emits a Biology boson ($B_b = \hbar\omega$) to $e_2$ losing the momentum $K$ and occupies the position of the hole ($h$) one ($h_1$) with momentum $P$. Then, $e_1$, through the Tunnel Effect, passes through the barrier (NH--N) to the position of $e_3$, where there is now a hole. Please check Figure 4 in the reference [8].

The first Josephson Equation $I_s = I_0.sin\ sin\ (\emptyset_2 - \emptyset_1)$ describes how the tunneling current depends on the two superconductors' phase difference. The second Josephson equation $\frac{d}{dt}(\emptyset_2 - \emptyset_1) = \frac{qV}{\hbar}$ represents the time evolution of the phase difference given an external voltage [11]. $V$ is the potential difference in JJ. These two equations describe the temporal phase evolution of the two superconductors. If a constant voltage is applied to a JJ, the phase difference will evolve linearly in time (AC current). As opposed, if we use no external voltage, the phase difference becomes constant (constant supercurrent despite no external voltage) due to the phase coherence of the pairs. It is known as the DC Josephson Effect.

If $\emptyset = \emptyset_2 - \emptyset_1$, then

$I_s = I_0.sin\ sin\ (\emptyset)$ Y $V = \frac{h}{4\pi e}\frac{d\emptyset}{dt}$

$P = \frac{dE_{jj}}{dt}$ with $E_{jj} = \int Pdt = \int VI_s dt = \int \frac{h}{4\pi e}\frac{d\emptyset}{dt}\ I_0.sin\ sin\ (\emptyset)\ dt$

Then, $E_{jj} = \frac{h}{4\pi e}\ I_0\ cos\ cos\ \emptyset$, where $E_j = \frac{h}{4\pi e}\ I_0$

Then, $cos\ cos\ \emptyset = 1 - \frac{1}{2}\emptyset^2 - \frac{1}{4!}\emptyset^4 + O(\emptyset^6)$

The first term $E_j$ can be disregarded because it is a constant factor while the terms of order $O(\emptyset^6)$ can be disregarded because of being $\emptyset$ small.

The Hamiltonian is an energy operator containing kinetic energy $K = \frac{P^2}{2m}$, and a potential energy of the form $V(r)$.

Them, $H = \frac{P^2}{2m} + V(r)$

The Hamiltonian of a qubit with a single JJ is given by

$$H = \frac{Q^2}{2C} + U(\Phi) \text{ with } U(\Phi) = \frac{\Phi^2}{2L} - E_j\ cos\ cos\ \left[\frac{2\pi}{\Phi_0}(\Phi - \Phi_{ext})\right]$$

$$\emptyset = 2\pi\frac{\Phi}{\Phi_0}$$

$n = \frac{Q}{2e}$ and $E_C = \frac{e^2}{2C}$

$$H = \frac{Q^2}{2C} + \frac{\Phi^2}{2L} - E_j\ cos\ cos\ \left[\frac{2\pi}{\Phi_0}(\Phi - \Phi_{ext})\right]$$

$H = 4E_C n^2 + E_j\left(\frac{1}{2L} + \frac{4\pi}{{\Phi_0}^2}\right)\Phi^2 + E_j\frac{2}{3{\Phi_0}^4}\Phi^4$ (1)

$\Phi$: flow in the JJ

$\Phi_{ext}$: external magnetic flux, $\Phi_{ext} = 0$

$C$: capacitance

$L$: Inductance

$E_j$: Josephson energy

$\Phi_0$: magnetic flux quantum

$E_{jj}$: JJ energy

Equation 1 is the Hamilton equation. Following the first quantization procedure, the two conjugate variables $n$ and $\Phi$ are promoted to non-commuting operators

$n = \hat{n}$ y $\Phi = \hat{\Phi}$

$\hat{H} = 4E_C\hat{n}^2 + E_j\left(\frac{1}{2L} + \frac{4\pi}{{\Phi_0}^2}\right)\hat{\Phi}^2 + E_j\frac{2}{3{\Phi_0}^4}\hat{\Phi}^4$ (2)

Preprints.org (www.preprints.org) | NOT PEER-REVIEWED | Posted: 25 September 2024 doi:10.20944/preprints202409.1016.v2



The first two terms in Equation 2 represent harmonic oscillators, and the third is the anharmonicity.

Introducing the standard annihilation $\hat{a}^-$ and creation $\hat{a}^+$ operators is useful.

$$\hat{a}^+ = \frac{1}{\sqrt{2}}\left(\frac{1}{\sqrt{\beta}}\hat{\Phi} + i\sqrt{\beta}\hat{n}\right)$$

$$\hat{a}^- = \frac{1}{\sqrt{2}}\left(\frac{1}{\sqrt{\beta}}\hat{\Phi} - i\sqrt{\beta}\hat{n}\right)$$

With $\beta = \sqrt{8\frac{E_C}{E_{j^*}}}$ where $E_{j^*} = \frac{1}{2}\left(\frac{1}{L} + \frac{8\pi}{{\Phi_0}^2}\right)E_j$

The action of $\hat{a}^+$ is to create a quantized excitation of the flux and charge degrees of freedom of the magnetic and electric fields. It creates a photon of frequency $\omega_r$ stored in the circuit.

In function of $\hat{a}^+$and $\hat{a}^-$:

$\hat{\Phi} = \sqrt{\frac{\beta}{2}}(\hat{a}^- + \hat{a}^+)$ and $\hat{n} = \frac{i}{\sqrt{2\beta}}(\hat{a}^- - \hat{a}^+)$

Then, the Hamiltonian in Equation 2 combines in:

$\hat{H} = \omega_r\left(\hat{a}^+\hat{a}^- + \frac{1}{2}\right) + \frac{\alpha}{12}(\hat{a}^+ + \hat{a}^-)^4$ (3)

With $\omega_r = \sqrt{8E_C E_{j^*}}$ the new frequency and the anharmonicity $\alpha = -E_C$

Please note that the Hamiltonian represented in Equations 2 and 3 corresponds to our qubit proposal based on the DNA characteristics and differs from those described in other works (Figure 2B).

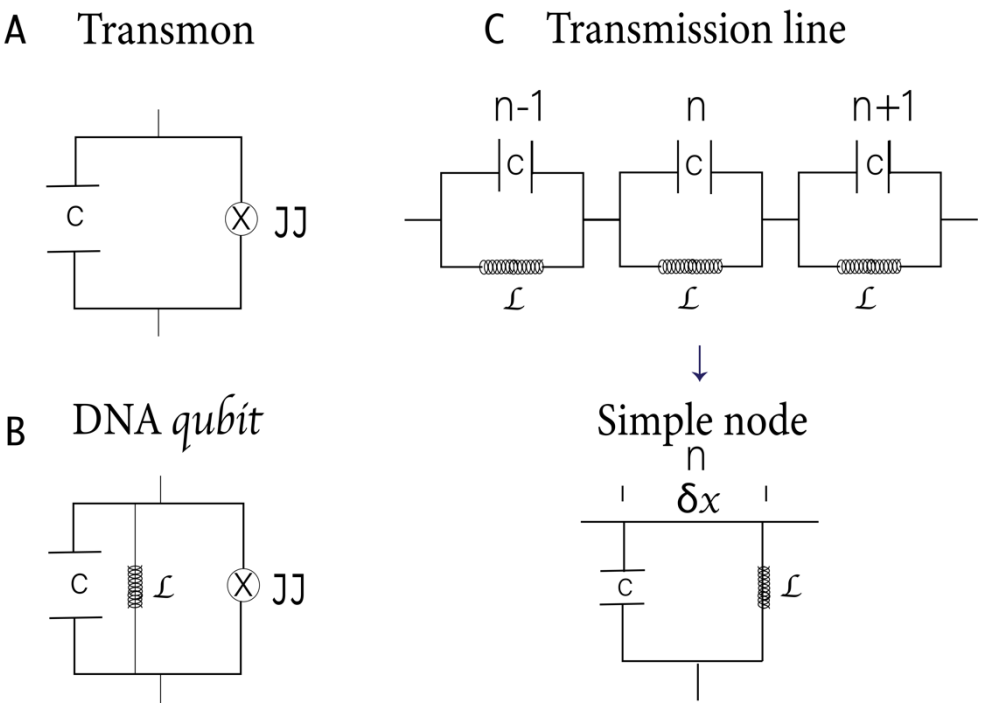


**Figure 2. Graphic representation of two qubits and two transmission lines**: A) Trasmon. B) DNA qubit. $C$ indicates the capacitor capacity, $L$, the inductance, and $\otimes$ the Josephson Junction. C) A typical finite transmission line with n-1, n, and n+1 nodes. A single node is represented.

## 4. DNA Backbone as a Finite Transmission Line with Distributed Parameters—The Hamiltonian Scheme

A transmission line is a structure of uniform geometry used to transport electrical signals or RF energy efficiently from one point to another [11]. It is also a medium that propagates information through electromagnetic waves at very high frequencies [42]. Because it behaves like a cable that spreads energy, it can be analyzed like a quantum oscillator electrical circuit based on its frequency response. The circuit is considered a line with distributed parameters at high frequencies since it has

 doi:10.20944/preprints202409.1016.v2



dimensions comparable to the wavelength [43]. Thus, the circulated current's amplitude and phase differ at every point. The wavelength is very short for high frequencies, so the transmission lines behave like resonant circuits for a specific frequency range.

Two parallel conductors form pair lines. Its various variants are used in telephony and data transmission [44,45]. Electromagnetic energy propagates around the conductors of the line. If a voltage $Vs$ is applied to a pair line, an electric $(E)$ field is generated between the conductors as opposite charges accumulate. The $Vs$ makes an electric current $(I)$ flow through the line's conductors terminated at a load impedance $(Z_L)$. This current also generates a magnetic $H$ field around the conductors. The direction of the current and fields is reversed in each half-cycle of the voltage [45]. By multiplying $H$ by $\mu$, we obtain the induction magnetic vector $(B)$, and then, by integrating $B$ over a plane parallel to the wires, we get the magnetic flux $(\Phi)$ that "joins" the circuit.

The mathematical definition of a circuit inductance is $L = \frac{\Phi}{I}$. If we have a transmission line length $x_0$ units long, and if that line has a distributed inductance $L$, then the inductance is just $L = Lx_0$. Two conductors with charge $\pm Q$ separated by a distance generate a potential difference $(V)$. $Q = \pm(\rho x_0)$ in every section of a transmission line length $x_0$. Where $\rho$ is the lineal distribute charge. The basic transmission line parameters are its capacitance (C) and inductance (L) per unit length, the impedance $(Z_0)$, and the mode frequency $(\omega)$ [21]. These parameters are related by:

$$Z_0 = \sqrt{\frac{L}{C}} \text{ and } \omega = \frac{1}{\sqrt{LC}}$$

The electric and magnetic fields are transverse to the direction of propagation. It is called Transverse Electromagnetic Waves (TEM) [46]. We can distinguish between infinite, semi-finite, and finite transmission lines. The latter is obtained by interrupting the central cable at two points so that a resonator that supports a quantized electromagnetic mode behaving like a harmonic oscillator is obtained. A resonator is a structure that encloses oscillatory electromagnetic energy without spreading it [11]. Boundary conditions restrict the wave configuration inside to patterns with integral numbers of half or quarter wavelengths along a propagation axis [45]. Therefore, specific discrete resonant frequencies $\omega_n$ are allowed. There is no energy dissipation if the resistive element is in series at zero current or parallel at zero voltage. Typical TEM resonators contain lossless elements at their end. Resonators are widely used to manipulate signals and energies, acting as bandpass filters allowing only frequencies close to the desired resonant frequency $(\omega_n)$ or as bands-stop filters letting all frequencies pass [21].

Characterizing single-stranded DNA as a transmission line is also of great interest. Single-stranded DNA can exhibit rich electrical properties. In the DNA backbone (formed by phosphate groups and deoxyriboses), C-N bonds attached deoxyriboses to the bp [47]. The negative charges at the phosphate groups connect the base pairs and give structural support for the double helix. Small polarons assisted hopping between the next nearest neighbors of the DNA molecular wire was suggested as the transport mechanism responsible for the solid high-temperature dependence of the electrical conductivity [48]. Our DNA wire model has connections between successive base pairs, the only sites included. Porath and Cols demonstrated that the sugar-phosphate backbones nor the specific bp sequence mediate the long-distance conduction in DNA [49]. Besides the multiple efforts to study the electrical current through single DNA fragments, the conduction mechanism, especially in long DNA molecules, is far from being established.

Figure 2C shows a schematic representation of DNA based on the model of parameters distributed in a transmission line. The line length is proportional to the total capacitance and inductance. In this model, the backbone phosphate groups carry the inductive effect, while the bases have the capacitive effect. Since it is a superconducting circuit, we will ignore the electrical resistance and magnetic fields within the strands, which are expelled due to the Meissner effect [8,50].

Using the Telegrapher equations, we can obtain the transmission line equation and assume the DNA strand acts as a lossless line with $R = 0$ and $G = 0$, where R and G are the resistance and shunt admittance per unit length [51]. The first equation

$$\frac{\partial V(x,t)}{\partial x} = -\left(L\frac{\partial I(x,t)}{\partial t}\right)$$

Preprints.org (www.preprints.org) | NOT PEER-REVIEWED | Posted: 25 September 2024 doi:10.20944/preprints202409.1016.v2



explains the voltage dependence the distributed inductance $L$ multiplied by the time derived from the current flowing in the line at one point. The second equation

$$\frac{\partial I(x,t)}{\partial x} = -\left(C\frac{\partial V(x,t)}{\partial t}\right)$$

explains that the current loss as we go down the line is proportional to the distributed capacitance $C$ multiplied by the time rate of the voltage change in the line.

An LC oscillator is characterized by its inductance L, capacitance C, angular frequency $\omega_r = \frac{1}{\sqrt{LC}}$, and impedance $Z_r = \sqrt{\frac{L}{C}}$. The oscillator energy is given by:

$$H_{LC} = \frac{Q^2}{2C} + \frac{\Phi^2}{2L} \quad (4)$$

As $I = \frac{dQ}{dt}$, and $Q(t) = \int_0^t I(t^*)d(t^*)$. Then,

$$H_{LC} = \frac{Q^2}{2C} + \frac{1}{2}CW_r{}^2\Phi^2 \quad (5)$$

Where by Faraday's law:

$$\Phi(t) = \int_0^t V(t)d(t)$$

Equation 5 is an LC harmonic oscillator equivalent to the coordinate mechanical harmonic oscillator $\Phi$

$$P = Q \text{ and } M = C$$

Then, $[\Phi, Q] = i\hbar$

Introducing the creation and annihilation operators ($\hat{a}^+$and $\hat{a}^-$)

$\hat{\Phi} = \Phi_{zpf}(\hat{a}^+ + \hat{a}^-)$ and $\hat{Q} = iQ_{zpf}(\hat{a}^+ - \hat{a}^-)$ with

$\Phi_{zpf} = \sqrt{\frac{\hbar}{2W_rC}} = \sqrt{\frac{\hbar Z_r}{2}}$ and $Q_{zpf} = \sqrt{\frac{\hbar W_rC}{2}} = \sqrt{\frac{\hbar}{2Z_r}}$. Then,

$$\hat{H}_{LC} = \hbar W_r\left(\hat{a}^+\hat{a}^- + \frac{1}{2}\right)$$

Where $\hat{a}^+\hat{a}^-|n\rangle = n|n\rangle$ with $n = 0,1,2,$ ...and $\frac{1}{2}$ is the zero-order energy or null energy.

$\hat{a}^+ = \sqrt{\frac{\hbar Z_r}{2}}\left(\hat{\Phi} - iZ_r\hat{Q}\right)$ creates a quantum excitation of flow and charge equivalent to the electric and magnetic Fields (a frequency photon $\omega_r$ inside the circuit).

We can generalize the result for a transmission line in the x direction and length d. The energy associated with each capacitor is $\frac{Q_n{}^2}{2C_0}$, and to each inductor $\frac{(\Phi_{n+1}-\Phi_n)^2}{2L_0}$. Where $\Phi_n$ is the variable flow associated with node n and $Q_n$ the conjugate variable is the charge at node n.

Then, the Hamiltonian for the discrete linear transmission resonator associated with Figure 2C is

$$H = \sum_{n=0}^{N-1}\left[\frac{1}{2C_0}Q_n{}^2 + \frac{1}{2L_0}(\Phi_{n+1} - \Phi_n)^2\right]$$

$L_0$and $C_0$: the variable inductance and capacitance associated with each node n and flow $\Phi_n$.

In the continuous limit, considering $\delta_x$ the size of a unit cell that tends to zero:

$C_0 = \delta_x c_0$ and $L_0 = \delta_x l_0$ with $c_0$ y $l_0$ the linear density of capacitance and inductance.

Defining a continuous flow field as $\Phi(x_n) = \Phi_n$ and the charge $Q(x_n) = \frac{Q_n}{\delta_x}$. Taking the $\delta_x$ and $d = N\Delta X$ constant, the Hamiltonian for a continuous linear transmission resonator:

$$H = \int_0^d dx\left[\frac{1}{2c_0}Q^2(x) + \frac{1}{2l_0}(\partial_x\Phi_x)^2\right] (6)$$

Where $\partial_x\Phi_x = \frac{(\Phi_{n+1}-\Phi_n)}{\delta_x}$

The charge $Q(x,t) = c_0\partial_t\Phi(x,t)$ is the generalized canonical moment of the flow $\Phi(x,t) = \int_0^t V(x,t)dt$ with $V(x,t)$ the voltage.

Using the information above, we obtain the wave propagation equation along the linear transmission resonator

$$v_0{}^2\frac{\partial^2\Phi(x,t)}{\partial x^2} - \frac{\partial^2\Phi(x,t)}{\partial t^2} = 0 \quad (7)$$

$v_0{}^2 = \frac{1}{l_0c_0}$ It is the speed of light in the biological medium of DNA.

 doi:10.20944/preprints202409.1016.v2



The Equation 7 solution is expressed as a linear combination of normal nodes of a size $\frac{\lambda}{2}$.

$$\Phi(x,t) = \sum_{m=0}^{\infty} U_m(x)\Phi_m(t)$$

with $\ddot{\Phi}_m = -{\omega_m}^2\Phi_m$ a differential equation of an oscillating function in time at the frequency node $\omega_m$

$$U_m(x) = A_m \, cos \, cos \, (K_m x + \varphi_m)$$

with amplitude $A_m$, wave vector $K_m = \frac{\omega_m}{v_0}$, and phase $\varphi_m$.

The Hamiltonian given by Equation 6 can be expressed as a discrete Hamiltonian:

$$H = \sum_{m=0}^{\infty} \left[\frac{{Q_m}^2}{2C_r} + \frac{1}{2}C_r{\omega_m}^2{\Phi_m}^2\right] \quad (8)$$

This Hamiltonian (Equation 8) represents the sum of simple harmonic oscillators. With $C_r = dc_0$ as the total capacitance of the resonator and $Q_m = C_r\dot{\Phi}_m$ the conjugate charge $\Phi_m$.

Following the quantization procedure with the variables $\Phi_m$ and $Q_m$, we define the creation and annihilation operators:

$$\hat{\Phi}_m = \sqrt{\frac{\hbar Z_m}{2}}\left({\hat{a}_m}^+ + {\hat{a}_m}^-\right)$$

$$\hat{Q}_m = i\sqrt{\frac{\hbar}{2Z_m}}\left({\hat{a}_m}^+ - {\hat{a}_m}^-\right)$$

Where $Z_m = \sqrt{\frac{L_m}{C_r}}$ the characteristic impedance of the m node and $\frac{1}{L_m} = C_r{\omega_m}^2$.

Then, the Hamiltonian given in Equation 8 finally transforms into:

$$\hat{H} = \sum_{m=0}^{\infty} \hbar\omega_m{\hat{a}_m}^+{\hat{a}_m}^-$$

With $\omega_m = (m+1)\omega_0$, and $\frac{\omega_0}{2\pi} = \frac{v_0}{2d}$ is the frequency.

## 5. DNA as a Quantum Electrodynamic Circuit—The Hamiltonian Scheme

A coplanar waveguide's (CPW) geometry allows for increased electromagnetic energy density and coupling [20]. The strong coupling permits operations to be carried out on the qubit and even entanglement of multiple qubits in the same cavity. Using two-dimensional CPWs (TD-CPWs) and circuit QED, researchers have realized high-efficiency entanglement up to 20 qubits and high-fidelity two-qubit gates for achieving up to 64 qubits. The electromagnetic field inside conventional superconducting resonators in circuit QED, (including TD-CPWs and 3D-cavities), are standing waves determined by boundary conditions, resulting in a topographic dependence of the fields' amplitude [21]. In circuit QED, resonant microwave cavities are replaced by sections of microwave transmission lines (integrated circuits) [19]. If superconducting materials are used, the system's losses and dephasing would be limited only by the system properties [11]. Another way to mitigate losses is to lower the electric field energy stored at interfaces and surfaces to the energy stored in a vacuum. That is why using 3D-microwave cavities or 3D- resonators rather than planar circuits is preferred [17,52]. This is a new quantum information processing prototype with information stored in a cavity.

Here, the effective Hamiltonian for our DNA archetype can be represented as

$$H = H_{RF-S} + H_{R1} + H_{R2} + H_{I_{RFS-R_1-R_2}} + H_\kappa + H_\gamma$$

Where, $H_{RF-S}$ is the Hamiltonian of a flux qubit with a single JJ (A-T, T-A, G-C, or C-G). $H_{R1}$ and $H_{R2}$ represented the Hamiltonian of the two single-stranded DNA separately. To complete the effective representation of the Hamiltonian in DNA, $H_{I_{RFS-R_1-R_2}}$ represents the interaction between the qubit and two-stranded DNA.

$H_\kappa$, the cavity losses, and the decay rate.

$H_\gamma$, decoherence, or decay of the two-level system.

As A-T and C-G are superconductors, their properties would limit the system's losses and dephasing ($H_\kappa = H_\gamma = 0$).

Preprints.org (www.preprints.org) | NOT PEER-REVIEWED | Posted: 25 September 2024 doi:10.20944/preprints202409.1016.v2



According to the Hamiltonian, a strong coupling qubit-cavity produces a special footprint when entry into resonance. The coherent oscillation between two quantum states is known as Rabi oscillation and the frequency as the Rabi frequency $\Omega_R$ (Figure 3). The $\Omega_R$ is proportional to the energy of the TLS-electromagnetic field interaction [53]. For a flux qubit coupled to a single mode of the electromagnetic field of a transmission line that acts as a resonator, the system's Hamiltonian consists of three parts: the qubit term ($H_1$), the electromagnetic field term confined in the resonator ($H_2$), and the Rabi-type interaction term ($H_3$).

$$\hat{H} = \hat{H}_1 + \hat{H}_2 + \hat{H}_3 = \frac{1}{2}(\epsilon(t)\sigma_z + \Delta\sigma_x) + \hbar\omega_r\left(\hat{b}^+\hat{b}^- + \frac{1}{2}\right) + \hbar g\sigma_y\left(\hat{b}^+ + \hat{b}^-\right) \quad (9)$$

$\omega_r$ resonator resonance frequency.

$\epsilon(t) = \epsilon_0 + A\,cos\,cos\,\omega t$ , but in DNA under the ground conditions $A\,cos\,cos\,\omega t = 0$. At this point, we consider the oscillator at a fixed instant.

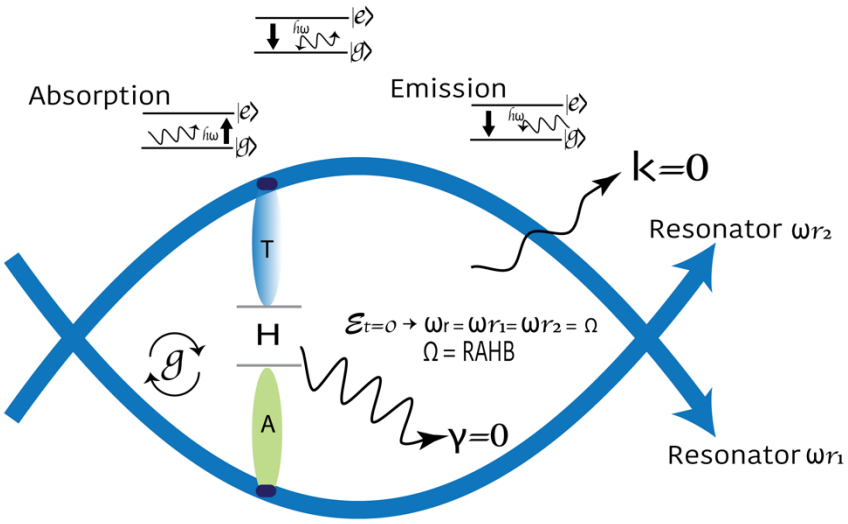


**Figure 3. Model of DNA as a 3D nonperturbative cavity quantum electrodynamics defined by two resonators**. In the zero-detuning case, a qubit is strongly coupled to a cavity and produces a unique signal when tuned into resonance. We hypothesize that the H-bond provides maximum coupling. RAHB: the resonance-assisted hydrogen bond. The Jaynes-Cummings Hamiltonian assumes the rotating wave approximation ($g \ll \omega_r, \Omega,\ \omega_r \sim \Omega$). The speed of quantum operations is represented by $g$. To maximize and maintain the coupling $g/\pi$ larger than the two main dephasing rates of the system $(g \gg k, \gamma)$ is the target.

Where $\epsilon_0$corresponds to the minimum energy or the fundamental state ($\epsilon_0 = \frac{1}{2}\hbar\omega$)

$\Delta$ corresponds to the two-level difference in energy for $\epsilon(t) = \epsilon_0,\ \Delta = \hbar\Omega_R$

$$\hat{H} = \frac{\hbar\Omega_R}{2}\sigma_x + \hbar\omega_r\left(\hat{b}^+\hat{b}^- + \frac{1}{2}\right) + \hbar g\sigma_y\left(\hat{b}^+ + \hat{b}^-\right)$$

In the absence of damping, the Hamiltonian can be readily diagonalized. The detuning parameter is $\epsilon(t) = \Omega_R - \omega_r$. In the zero-detuning case $\Omega_R = \omega_r$.

$\sigma_x$, $\sigma_y$ and $\sigma_z$ are the Pauli matrices.

$\hat{b}^+$ and $\hat{b}^-$photon creation and annihilation operators.

$g$ Intensity of the qubit-electromagnetic field coupling rate. It depends on the strength of the electric or magnetic field at the system site, its dipole moment, and the system's properties [52].

$$g = \frac{dA_e}{\sqrt{2}\hbar} \text{ or } g = \frac{\mu A_m}{\sqrt{2}\hbar} \quad (10)$$

where $A_e$ and $A_m$ are the electric and magnetic field amplitudes.

Expanding the interaction term in terms of the rise and fall operators $\sigma_y = \sigma_+ + \sigma_-$

$$\hbar g\left(\sigma_+\hat{b}^+ + \sigma_+\hat{b}^- + \sigma_-\hat{b}^+ + \sigma_- + \hat{b}^-\right)$$

A TLS and a harmonic oscillator are coupled in a circuit QED [21]. The circuit can operate in two limits: on-resonant and off-resonant dispersive regimes. On resonance, the separation between the

 doi:10.20944/preprints202409.1016.v2



two energy levels of the qubit resonates with the transmission line frequency. Entangled qubit-photon states are generated, and both system parts can exchange excitations without energy loss [11]. In an ultra-strong coupling regime, the coupling intensity reaches values comparable to the resonator frequency, rendering the Jaynes-Cummings Model invalid. In the dispersive regime, the transmission line frequency differs from the qubit energy levels separation. In this situation, the energy levels of the qubit will depend on the photons and vice versa. Consequently, the resonator could obtain information about the qubit's state and couple multiple qubits together [54].

Molecular circuits have been developed to control complex functions in biological and biochemical systems. In the DNA ground state, each nitrogenous base is coupled to a transmission line in resonance with the H-bond that joins it to its complementary base connected to a second transmission line. When RNA pol II emits pulses at the end of the transmission line, the system enters a dispersive regime. It is a sub-regime of the Jaynes-Cummings Model that allows measurements of the qubit's state acting on the resonator. The energy levels of the qubit are normalized depending on the state of the resonator and vice versa [54]. The qubit state is determined by varying the waveguide frequency until it matches the new frequency of the resonator. It also allows manipulation of the qubit by forcing the resonator with a signal sent through the waveguide similar to the natural qubit frequency.

This work approaches the DNA gene structure as the lineal combination of circuits-QED. Each qubit level of a flux qubit is coupled to an independent resonator. The frequency of the qubit is similar to that of the resonators it has been connected to. For a flux qubit coupled to two modes of the electromagnetic field of a transmission line that acts as a resonator, the system's Hamiltonian consists of three parts: the qubit term ($H_1$), the electromagnetic field term confined in the two resonators, and the Rabi-type interaction term ($H_2$). (modified from Equation 9):

$$\widehat{H} = \widehat{H}_1 + \widehat{H}_2 = \frac{1}{2}(\epsilon(t)\sigma_z + \Delta\sigma_x) + \sum_{i=1}^{2} \left( \hbar\omega_{r_i} \left( \hat{b}_i^{+} \hat{b}_i^{-} + \frac{1}{2} \right) + \hbar g_i \sigma_y \left( \hat{b}_i^{+} + \hat{b}_i^{-} \right) \right)$$

In the DNA ground state, $\epsilon(t) = \Omega_R - \omega_r = o$

$$\widehat{H} = \frac{\hbar\Omega_R}{2}\sigma_x + \sum_{i=1}^{2} \left( \hbar\omega_{r_i} \left( \hat{b}_i^{+} \hat{b}_i^{-} + \frac{1}{2} \right) + \hbar g_i \sigma_y \left( \hat{b}_i^{+} + \hat{b}_i^{-} \right) \right)$$

In DNA, A-T, T-A, C-G, and G-C qubits are coupled to a virtual cavity defined by two resonators. This constitutes the DNA basic unit. The difference between the system's energy levels in the DNA ground state is $\hbar\Omega_R$ due to the movement of electron and hole pairs in the aromatic ring without an external force [8]. A-T and C-G are strongly coupled to the resonators, which allow operations to be performed during the lifetime of the quantum state. The coherent oscillation between the two bp quantum states is equivalent to the phenomenon known as Rabi oscillations. The oscillation frequency is the Rabi frequency. It is related to the energy of the qubit-electromagnetic field interaction. A perturbation can tune the bp levels such that a certain level splitting coincides with the cavity photon energy Figure 4.

Preprints.org (www.preprints.org) | NOT PEER-REVIEWED | Posted: 25 September 2024 doi:10.20944/preprints202409.1016.v2



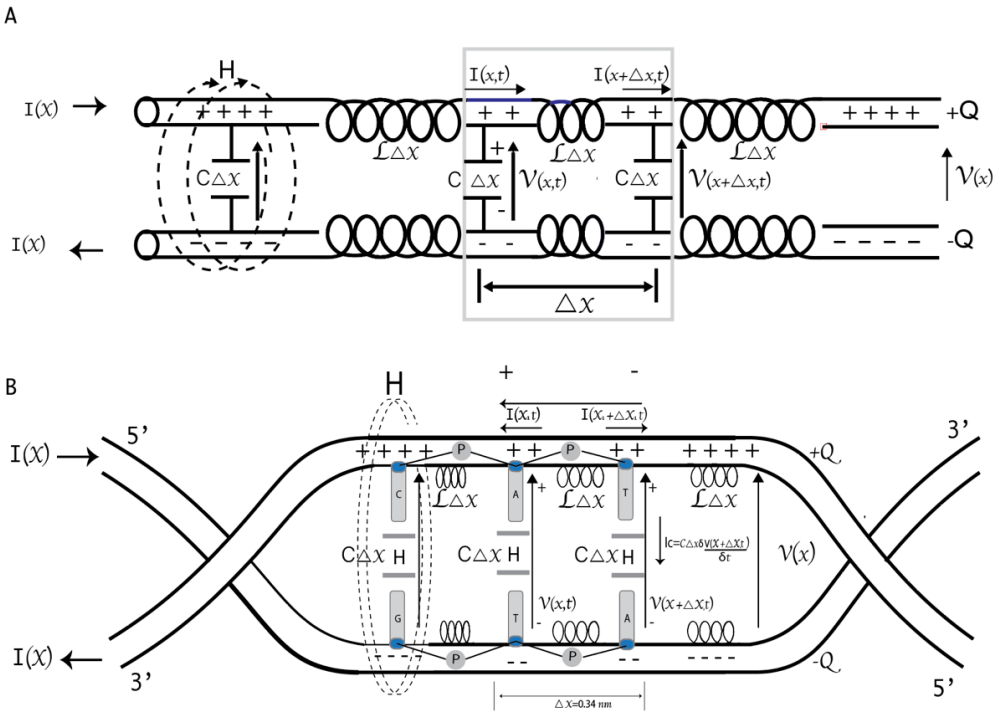


**Figure 4. Model of DNA strands as a distributed parameter transmission line**. A) Representation of the distributed inductance and capacitance in a transmission line. The line is divided into $\Delta x$ sections, each with an inductance $L\Delta x$ and capacitance $C\Delta x$. B) Representation of the distributed inductance and capacitance in DNA strands as transmission lines. There are connections between successive bp. Hence the distributed sites are the nucleobases. Each level of the DNA qubit is capacitively coupled to a transmission guide, subject to harmonic forcing in the magnetic flux passing through it. The application of Kirchhoff's laws is represented.

Analyzing Equation (10), the average field strength is estimated using the integral of the field amplitude over the space volume delimited by the two resonators. DNA spiral diameter is around 2 nm. Thus, we assume that the space dimensions give us $V = \frac{4}{3}\pi r^3$, where $V$ is the sphere´s volume, and $r$ is the radio. Taking a space average and setting that $\epsilon = \epsilon_0$ and $\mu = \mu_0$ [52]:

$$\frac{1}{2}\int \epsilon |A_e|^2 dV = \frac{\hbar\omega_r}{2} \text{ or } \frac{1}{2}\int \frac{|A_m|^2}{\mu} dV = \frac{\hbar\omega_r}{2}$$

$$\frac{1}{2}\epsilon_0 A_e^2 V = \frac{\hbar\omega_r}{2} \text{ or } \frac{1}{2\mu_0} A_m^2 V = \frac{\hbar\omega_r}{2}$$

$$\frac{2}{3}\epsilon_0 A_e^2 \pi r^3 = \frac{\hbar\omega_r}{2} \text{ or } \frac{2}{3\mu_0} A_m^2 \pi r^3 = \frac{\hbar\omega_r}{2}$$

$$A_e^2 = \frac{3\hbar\omega_r}{4\pi\epsilon_0 r^3} \text{ or } A_m^2 = \frac{3\mu_0\hbar\omega_r}{4\pi r^3}$$

Then, $A_e = \frac{1}{2r}\sqrt{\frac{3\hbar\omega_r}{\pi\epsilon_0 r}}$ for the electric field and $A_m = \frac{1}{2r}\sqrt{\frac{3\mu_0\hbar\omega_r}{\pi r}}$ for the magnetic fiel.

In the following section, we will describe the theoretical basis for DNA Transcription and compare this process to the dispersive detuning regime.

## 6. Quantum Description of Transcription

Despite the progress in elucidating the critical events during transcription, what needs to be addressed is that the process takes place strictly in a spatially defined manner. How the transcription spatial organization is achieved is still an unsolved question. A physiochemical phenomenon called biomolecular condensates is partly formed through phase separation to achieve spatiotemporal regulation of some biological processes [55–58]. The phase separation is crucial in regulating the transcriptional events in every step of a transcription cycle (Figure 1A) [59,60].

 doi:10.20944/preprints202409.1016.v2



Multivalent interactions constitute driving forces underlying phase separation in biomolecular condensates. They include disordered regions and structured, repeated modular oligomerization domains [61]. Some molecules function as scaffolds to assemble phase-separated structures, whereas client components are recruited by directly binding to scaffolds [55]. In general, modular interaction domains in evolutionarily conserved protein segments create multivalency that facilitates the engagement of multiple binding complexes. The dynamic interacting networks initiate and promote phase separation [60]. In many proteins, the succession of structural components such as tyrosine, glycine, and serine have provided multivalency to undergo phase separation and enable the formation of biomolecular condensates [29]. Unlike the classical transcription describing the RNA pol II tracks along the relatively static DNA template strand to synthesize the nascent RNA, the phase separation model allows for the description of a quantum model of transcription. RNA pol II can be incorporated into transcriptional condensates [58,61]. Transcription bubble translocation along the DNA requires rotation of the RNA pol around the DNA axis. The linking number density has been calculated using the equation:

$$\omega_0 x = \theta + \emptyset \text{ with } \omega_0 = 1.85\, nm^{-1}$$

Where $\omega_0 x$ is the accumulative rotational angle, $x$ is the distance in $nm$, $\theta$ is the RNA pol rotation angle, and $\emptyset$ the DNA rotation at the RNA pol site. Based on DNA supercoiling-transcription interplay, experiments have shown the maximum RNA pol II translocation rate or velocity is $\upsilon_0 = 20\, nm.s^{-1} \approx (60\, bp).s^{-1}$. [26].

The ability of pol II as the scaffold for the PIC arises from its CTD, which is flexible and highly disordered. CTD and phase separation close relationship is vital in initiating efficient transcription. The role of CTD-P in activating co-transcriptional capping is well-established [31]. The favorable regulation of CTD in condensates is reversibly controlled depending on CTD-P [29]. It determines pol II positioning into different condensates as transcription progresses. For example, the transition between initiation and elongation is associated with $Kin_{28}$-mediated $Ser_5$-P within the heptapeptide repeats [27]. Hence, it raises an essential question of whether P is the transcription's driving pulse.

In P-reactions, the side chain hydroxyl groups on specific proteins' serine, threonine, and tyrosine residues are modified with the gamma phosphate, producing a theatrical change in the protein's architecture and function [62]. ATP is almost always the phosphate donor [63]. It can be represented as A-P~P~P, where °~°°~° are the high-energy acid anhydride bonds. One of those is hydrolyzed. Breaking these bonds is an endergonic process that consumes energy rather than releasing it [64,65]. The negative change in the Gibbs free energy is due to the bonds formed after the hydrolysis process having a lower energy than before. The new bonds in hydrolysis allow the release of enormous energy, exactly 7.7 kcal/mol: ΔG= -7,7 kcal/mol o -31 KJ/mol [66].

Unlike most biological processes in which only one phosphate group ($P_i$) is separated, the last two phosphate groups are released in the form of the pyrophosphate group ($PP_i$) in replication. This process can be summarized in a chemical equation:

$$(DNA)_n + dNTP \leftrightarrow (DNA)_{n+1} + PP_i \text{ [67].}$$

Similarly, during transcription elongation, the overall reaction equation:

$$(NMP)_n + NTP \leftrightarrow (NMP)_{n+1} + PP_i \text{ [68].}$$

The H-bond is a robust fixed dipole-dipole electrostatic force when many molecules join. It provides excellent stability but is weaker than the covalent or ionic bonds. The energy of a H-bond is typically 5 to 30 kJ/mol, but it can vary from very weak to very strong. For N—H...N, it is approximately 13 kJ/mol. Intermolecular H-bond is responsible for the high boiling point of water (100°C). ATP to ADP hydrolysis releases 30.5 kJ/mol, with a free energy change of 3.4 kJ/mol [66].

A transition between energy levels caused by forcing one of the system parameters' Hamiltonian is called a Landau-Zener transition. A series of successive Landau-Zener transitions occur when a TLS is subject to periodic forcing on one of its parameters with a sufficiently intense amplitude [69]. Detuning can be modified externally

$$\epsilon(t) = \epsilon_0 + A\, cos\, cos\, \omega_{ext} t$$

where $A$ and $\omega_{ext}$ are the forcing amplitude and frequency, respectively. The qubit levels are anti-symmetrically coupled

$$g_1 = -g_2, \text{ and } \epsilon_1(t) = -\epsilon_2(t).$$

Preprints.org (www.preprints.org) | NOT PEER-REVIEWED | Posted: 25 September 2024 doi:10.20944/preprints202409.1016.v2



The qubit eigenstates can be defined as $|\uparrow\rangle$, $|\downarrow\rangle$.

The dispersive detuning regime, where $\epsilon(t) \gg g$ is helpful in quantum computing because it allows quantum measurements of the qubit state and its manipulation [11]. Irradiating at the qubit frequency $\Omega$ handle the qubit coherently. Irradiating at the resonator frequency $\omega_r$ introduce photons in the cavity that become entangled with the qubit states. The law of conservation of linear momentum requires that at least two photons be created so that the resulting linear momentum can be equal to zero [46,70]. The photon is the gauge boson of the electromagnetic interaction and, therefore, is a boson that acts as a carrier of a fundamental interaction of nature. Conservation laws can determine the energies of the two photons or, equivalently, their frequencies. A driving radiation field of frequency $\omega_{ext}$ acting on the qubit-resonator system during a specific time can be described by the Hamiltonian [71]:

$$\hat{H}(t) = \hbar\,\Delta(t)\left(\hat{b}^{+}q^{-i\omega_{ext}t} + \hat{b}^{-}q^{i\omega_{ext}t}\right) \quad (11)$$

where $q$ is the electron charge.

Every qubit is represented as a point on the Bloch sphere, where the poles represent the eigenstates [72]. The colatitude angle, $\theta$, runs through the angles from 0 to $\pi$, while the azimuthal angle, $\phi$, runs from 0 to $2\pi$ [73]. The effect of a quantum gate on a single qubit is a rotation in the Bloch sphere, giving rise to a new qubit. In the Bloch sphere, we visualize the action of different logic gates or the temporal evolution of the state of a TLS described by a Hamiltonian. An axis and a rotation angle define a rotation operator [74]. Its action produces a rotation of the point on the sphere concerning the rotation axis at the rotation angle [73,75]. The relationship between the angle of rotation in the x-axis and the pulse parameters in the Bloch sphere is represented in the equation:

$$\theta(t) = \Omega V_0 \int_0^t f(t')dt'$$

Since the Rabi oscillations follow an expression of sin[2], we can obtain their period and determine the Rabi frequency and, even more importantly, the value of the variable parameter of the pulse makes it go from the state $|0\rangle$ to the state $|1\rangle$, a logic gate $\pi$ [75]. To perform rotations around the y-axis, multiply the pulse amplitude by the imaginary unit (a phase of $\emptyset = \frac{\pi}{2}$ that is added to the pulse).

$$U(t) = exp\ exp\left(-i\int_0^t H_d^I(t')dt'\right) = exp\left(\frac{i}{2}\Omega V_0\left(I\sigma_x - Q\sigma_y\right)\int_0^t f(t')dt'\right)$$

By combining Equation 11 with the Hamiltonian of the system in Equation 9 and applying the unitary transformation [52]:

$$\hat{U} = exp\left(\frac{g}{\epsilon(t)}\left(\hat{b}^{-}\sigma_{+} - \hat{b}^{+}\sigma_{-}\right)\right)$$

we get the single qubit Hamiltonian in the frame rotating at the driving radiation field of frequency $\omega_{ext}$ acting on the qubit-resonator system during a specific time:

$$\hat{H} = \frac{\hbar}{2}\left(\Omega + 2\frac{g^2}{\epsilon(t)}\left(\hat{b}^{+}\hat{b}^{-} + \frac{1}{2}\right) - \omega_{ext}\right)\sigma_z + \hbar\frac{g\Delta}{\epsilon(t)}\sigma_x + \hbar(\omega_r - \omega_{ext})\hat{b}^{+}\hat{b}^{-} + \hbar\Delta\left(\hat{b}^{+} + \hat{b}^{-}\right)$$

The current in a transmission line is proportional to the relationship between the voltage's magnitude and the line's impedance (I=V/Z). This simple Ohm's Law will hold for a transient period [76].

Three effects can generate a superconducting phase difference around the circuit [11].

1. Due to the Josephson effect. When the pairs coherently pass through a JJ, the supercurrent $I$ related to the phase difference between electrodes can be represented by $I = I_0\ sin\ sin\ \phi$. $I_0$ is the maximum critical current the junction can maintain. In our model of DNA, the maximum crucial current of the H-bond is $I_0$.
2. Due to the supercurrent, an intrinsic phase shift appears when computing the line integral of momentum $\vec{p}$ pairs moving along the curve.
3. Due to external magnetic flux. Classical electromagnetism and Maxwell's laws show that a magnetic field that changes with time induces an electric field. This, in turn, modifies the momentum of the charged particles by exerting a force on them. The moment of the electron

 doi:10.20944/preprints202409.1016.v2



pairs is given by equation $\vec{p} = 2m_e\vec{v} + 2e\vec{A}$. The first component corresponds to the kinetic part, and the second to the field contribution—the potential vector is $\vec{A}$.

In our DNA model, RNA pol II changes the external magnetic flux through a P-mechanism and generates a phase difference. RNA pol II sends the system pair of pulses with the same parameters many times (n). The total number of pulses required may explain why the enzyme's catalytic site has 52 repeats (Figure 1A). Then, the number of times (m) the system was in state $|0\rangle$ or $|1\rangle$ is extracted. With these data, the probability that the system is in a specific state is calculated by applying Laplace's rule. For example, to obtain the probability that it is in state $|0\rangle$: $P(|0\rangle) = \frac{m}{n}$. We can obtain the Rabi oscillations by representing the probabilities as a function of times. At a computational level, a pulse is a finite time series of complex values, where each value represents a pulse amplitude at a given time. In DNA, a pulse is a finite time series of P-reactions.

**7. Discussion**

The spin 1/2 particles are TLS useful for quantum computation. In the DNA ground state, the $\pi$-ring controlled the hyperfine and electron-mediated nuclear spin interactions. Previously, close connections between classical and quantum information were described in DNA [8]. In this work, we characterized A-T and C-G bp as flow qubits, as they constitute a superconducting ring interrupted by one JJ and crossed by a magnetic flux. Recent studies treated the H-bond between DNA bp as adiabatic systems with spin-orbit coupling. Hubač and Cols. extensively defined qubits formed by Majorana fermions in the H-bond and discussed the entangled states in the bp [78]. The Hamiltonian obtained in this work for the DNA qubits differs from that of the transmon. However, in the limit when L tends to be infinite (omitting the term $\frac{1}{2L}$ in Equation 2), our Hamiltonian (Figure 2B) tends to be the transmon Hamiltonian (Figure 2A).

In DNA, each bp is connected to the adjacent by the sugar-phosphate backbone. This structure is similar to a transmission line with distributed parameters. Changes in the magnetic field by the RNA pol II during transcription could flip nuclear spins at resonance. An applied magnetic field breaks electrons' twofold spin degeneracy. A pulse set detuned from the resonant frequency and enables the state of the qubit to be determined. One question emerged: What is the energy to get the lowest donor-excited state? This work considers high intra-complex P-activity manifested in processive P-reactions of alcohol residues in RNA pol II using ATP as the phosphate donor as the RNA pol II driving force. Multisite P-networks emerge as a new level of signal based on routes encoded into disordered regions of proteins [79]. PPi release during transcription is a signature step in each nt addition cycle [68]. A DNA circuit can be represented as a symmetric and antisymmetric sin function: $y = A\,sin\,sin\,x$ and $y = -A\,sin\,sin\,x$. We proposed the graphic representation of the DNA strands' deformation due to the H-bond break to form the Bloch sphere. The rotations of the qubit are carried out during transcription (Figure 1B).

The coupling of each spin to its neighbors and the magnetic field enables numerous operations on each spin. Measurements are performed by determining the electron spin state effect on the electrons' orbital wavefunction after transferring nuclear spin polarization to the electrons [11]. Also, quantum computation requires a two-qubit controlled rotation proceeding. The result is a rotation of a target qubit when the control qubit is oriented in a specified direction and still unchanged [20]. The measurable signal decreases with the number of qubits [80]. Previous studies reported that more than ten qubits will be challenging. Looking at the spins inside a DNA loop, they are arranged in parallel. In principle, logical operations and measurements can be performed independently and in parallel on each spin in the array.

Circuit QED points to multiple superconducting qubits and 3D cavities with high coherence [21]. Distributed quantum computation arises across numerous single-mode resonators [20]. Single-step multi-qubit phase gates on multiple single-mode resonators mediated by a superconducting bus in circuit QED have been described [81]. The superconducting bus may be possible single-mode resonator interactions, and quantum information is encoded in various single-mode resonators' vacuum and single-photon states [11]. In addition, the pulse engineering technique adjusts the

 doi:10.20944/preprints202409.1016.v2



coupling strength between resonators and the bus enhancing fidelity and robustness. The tunable coupling strength plays a broad role in the circuit QED system [20].

Based on the above information, we consider that a DNA gene's basic structure is the nonperturbative circuit QED, and a complete gene would be the linear combination of $n$ circuits in parallel. This parallel arrangement, together with its superconducting nature, contributes to the total resistance being zero, and there is no heat dissipation. DNA gene transcription process includes the combination of $n$ cavities hosting nine qubits and coupled to a shared machine. Many qubits in a single cavity may increase the unwanted qubit-qubit interaction and the cavity decay while decreasing the qubit-cavity coupling strength [20,54,80]. Hence, multiple cavities and quantum operations on qubits distributed in different cavities are mandatory for large-scale quantum information processing.

The RNA pol II bus holds a level structure formed by ground and excited levels, denoted by $|g_1, g_2 \ldots g_n\rangle$ and $|e_1, e_2 \ldots e_n\rangle$, respectively. Adjusting the qubit level spacings achieves the coupling and decoupling of each qubit from its cavity. The P-pulses applied to the bus drive the transitions resonantly between $|e_x\rangle$ and $|g_{x+1}\rangle$ with Rabi frequency $\Omega_x$. Realizing quantum information transfer (QIT) and entanglement with SQUIDs in a microwave cavity is feasible in artificial atom models [82].

## 8. Conclusions

Biomolecular condensates concentrate functionally related components through multivalent and dynamic interactions in biopolymers without a bounding membrane. Using the transcription condensate architecture and the Electrodinamyc Quantum Theory of Circuits, we further developed ideas about the electrical design of quantum information in DNA. This Theory is an excellent model for characterizing the transcription process and describing the Hamiltonians that define the function in secondary quantification using the methods of Quantum Physics. In this work, we address the graphic and physical-mathematical representation of the DNA qubit as a nonlinear quantum circuit that introduces anharmonity through the H-bond. There are similarities between DNA qubits and RF-SQUIDs coupled to a cavity mode defined by two resonators. However, DNA qubits differ from the transmon qubits.

To characterize DNA as a transmission line or a wire model, the backbone structure of single-stranded DNA must be analyzed. It has connections between successive bp. Hence, the line's superconductors in a given gene are the bp. Each single DNA strand backbone works like a TEM with discrete distributed parameters. In this work, we described the Hamiltonian of one qubit coupled to two resonators. We concluded that every single gene in DNA can be modeled as a combination of $n$ circuit. The RNA pol II, acting like a multifunctional biomolecular machine, produces the system's decoherence like an artificially engineered device. A processive phosphorylation circuit with multiple kinase inputs and in the 52 repeated heptad motif ($Tyr_1Ser_2Pro_3Thr_4Ser_5Pro_6Ser_7$) controls multi-target qubits. The PPi release step is crucial to the mechano-chemical coupling mechanism during transcription elongation because it is equivalent to the computation pulse. The transcription process involves coupling n circuits, each containing nine qubits.

Evolutionarily conserved biological processes are critical and contain essential secrets that allow a specific function to be carried out. Knowing these deep secrets helps us understand fundamental human and natural development processes. Understanding basic quantum interactions is essential to discovering these biological secrets. Quantum Molecular Biology is an emerging and fascinating field of study. The quantum information in DNA is related to life evolution and preservation.

**Authors' contributions:** ARL conceived of the study. ARL and RRA performed mathematical theoretical analysis. ARL, RRA, YMOG, ECSM, JSEC, ACMS wrote the manuscript. All authors analyzed and discussed the data. All authors read and approved the final manuscript.

**Funding:** This research received no specific grant from any funding agency in the public, commercial, or not-for-profit sectors.

 doi:10.20944/preprints202409.1016.v2



**Declaration of competing interests:** There is no conflict of interest of any the authors with the results of this work.

## References


1. Nudler, E. RNA Polymerase Active Center: The Molecular Engine of Transcription. *Annu Rev Biochem* **78**, 335–361 (2009).
2. Martinez-Rucobo, F. W. & Cramer, P. Structural basis of transcription elongation. *Biochimica et Biophysica Acta (BBA) - Gene Regulatory Mechanisms* **1829**, 9–19 (2013).
3. Werner, F. & Grohmann, D. Evolution of multisubunit RNA polymerases in the three domains of life. *Nat Rev Microbiol* **9**, 85–98 (2011).
4. Vannini, A. & Cramer, P. Conservation between the RNA Polymerase I, II, and III Transcription Initiation Machineries. *Mol Cell* **45**, 439–446 (2012).
5. Lu, F. Several Ways to Implement Qubits in Physics. *J Phys Conf Ser* **1865**, 022007 (2021).
6. Basilewitsch, D., Schmidt, R., Sugny, D., Maniscalco, S. & Koch, C. P. Beating the limits with initial correlations. *New J Phys* **19**, 113042 (2017).
7. Fursina, A. A. & Sinitskii, A. Toward Molecular Spin Qubit Devices: Integration of Magnetic Molecules into Solid-State Devices. *ACS Appl Electron Mater* **5**, 3531–3545 (2023).
8. Riera Aroche, R., Ortiz García, Y. M., Martínez Arellano, M. A. & Riera Leal, A. DNA as a perfect quantum computer based on the quantum physics principles. *Sci Rep* **14**, 11636 (2024).
9. Dos Santos, C. S., Filho, E. D. & Ricotta, R. M. Quantum confinement in hydrogen bond of DNA and RNA. *J Phys Conf Ser* **597**, 012033 (2015).
10. Majer, J. et al. Coupling superconducting qubits via a cavity bus. *Nature* **449**, 443–447 (2007).
11. Clarke, J. & Wilhelm, F. K. Superconducting quantum bits. *Nature* **453**, 1031–1042 (2008).
12. Karamitros, D., McKelvey, T. & Pilaftsis, A. Quantum coherence of critical unstable two-level systems. *Physical Review D* **108**, 016006 (2023).
13. Linke, N. M. et al. Experimental comparison of two quantum computing architectures. *Proceedings of the National Academy of Sciences* **114**, 3305–3310 (2017).
14. Wen, C. P. Coplanar Waveguide: A Surface Strip Transmission Line Suitable for Nonreciprocal Gyromagnetic Device Applications. *IEEE Trans Microw Theory Tech* **17**, 1087–1090 (1969).
15. Bennett, R., Barlow, T. M. & Beige, A. A physically motivated quantization of the electromagnetic field. *Eur J Phys* **37**, 014001 (2016).
16. Sarabi, B., Ramanayaka, A. N., Burin, A. L., Wellstood, F. C. & Osborn, K. D. Cavity quantum electrodynamics using a near-resonance two-level system: Emergence of the Glauber state. *Appl Phys Lett* **106**, (2015).
17. Blais, A., Grimsmo, A. L., Girvin, S. M. & Wallraff, A. Circuit quantum electrodynamics. *Rev Mod Phys* **93**, 025005 (2021).
18. Hwang, M.-J. & Choi, M.-S. Variational study of a two-level system coupled to a harmonic oscillator in an ultrastrong-coupling regime. *Phys Rev A (Coll Park)* **82**, 025802 (2010).
19. Joo, J., Lee, C.-W., Kono, S. & Kim, J. Logical measurement-based quantum computation in circuit-QED. *Sci Rep* **9**, 16592 (2019).
20. Han, J.-X. et al. Multi-qubit phase gate on multiple resonators mediated by a superconducting bus. *Opt Express* **28**, 1954 (2020).
21. Blais, A., Girvin, S. M. & Oliver, W. D. Quantum information processing and quantum optics with circuit quantum electrodynamics. *Nat Phys* **16**, 247–256 (2020).
22. Travers, A. & Muskhelishvili, G. DNA structure and function. *FEBS J* **282**, 2279–2295 (2015).
23. Wing, R. et al. Crystal structure analysis of a complete turn of B-DNA. *Nature* **287**, 755–758 (1980).
24. Kohestani, H. & Wereszczynski, J. The effects of RNA.DNA-DNA triple helices on nucleosome structures and dynamics. *Biophys J* **122**, 1229–1239 (2023).
25. Wong, K. H., Jin, Y. & Struhl, K. TFIIH Phosphorylation of the Pol II CTD Stimulates Mediator Dissociation from the Preinitiation Complex and Promoter Escape. *Mol Cell* **54**, 601–612 (2014).
26. Tripathi, S., Brahmachari, S., Onuchic, J. N. & Levine, H. DNA supercoiling-mediated collective behavior of co-transcribing RNA polymerases. *Nucleic Acids Res* **50**, 1269–1279 (2022).
27. Mayfield, J. E. et al. Tyr1 phosphorylation promotes phosphorylation of Ser2 on the C-terminal domain of eukaryotic RNA polymerase II by P-TEFb. *Elife* **8**, (2019).
28. Boehning, M. et al. RNA polymerase II clustering through carboxy-terminal domain phase separation. *Nat Struct Mol Biol* **25**, 833–840 (2018).
29. Lu, H. et al. Phase-separation mechanism for C-terminal hyperphosphorylation of RNA polymerase II. *Nature* **558**, 318–323 (2018).
30. McNamara, R. P. et al. KAP1 Recruitment of the 7SK snRNP Complex to Promoters Enables Transcription Elongation by RNA Polymerase II. *Mol Cell* **61**, 39–53 (2016).

 doi:10.20944/preprints202409.1016.v2




31. Du, X. et al. RBM22 regulates RNA polymerase II 5′ pausing, elongation rate, and termination by coordinating 7SK-P-TEFb complex and SPT5. *Genome Biol* **25**, 102 (2024).
32. Turecka, K., Firczuk, M. & Werel, W. Alteration of the −35 and −10 sequences and deletion the upstream sequence of the −35 region of the promoter A1 of the phage T7 in dsDNA confirm the contribution of non-specific interactions with E. coli RNA polymerase to the transcription initiation process. *Front Mol Biosci* **10**, (2024).
33. Klein, C. A., Teufel, M., Weile, C. J. & Sobetzko, P. The bacterial promoter spacer modulates promoter strength and timing by length, TG-motifs and DNA supercoiling sensitivity. *Sci Rep* **11**, 24399 (2021).
34. Paget, M. S. & Helmann, J. D. The σ70family of sigma factors. *Genome Biol* **4**, 203 (2003).
35. Borukhov, S. & Nudler, E. RNA polymerase: the vehicle of transcription. *Trends Microbiol* **16**, 126–134 (2008).
36. Martinez-Rucobo, F. W., Sainsbury, S., Cheung, A. C. & Cramer, P. Architecture of the RNA polymerase-Spt4/5 complex and basis of universal transcription processivity. *EMBO J* **30**, 1302–1310 (2011).
37. Gnatt, A. L., Cramer, P., Fu, J., Bushnell, D. A. & Kornberg, R. D. Structural Basis of Transcription: An RNA Polymerase II Elongation Complex at 3.3 Å Resolution. *Science (1979)* **292**, 1876–1882 (2001).
38. Korzheva, N. et al. A Structural Model of Transcription Elongation. *Science (1979)* **289**, 619–625 (2000).
39. Xu, J., Chong, J. & Wang, D. Opposite roles of transcription elongation factors Spt4/5 and Elf1 in RNA polymerase II transcription through B-form versus non-B DNA structures. *Nucleic Acids Res* **49**, 4944–4953 (2021).
40. Yu, J., Retamal, J. C., Sanz, M., Solano, E. & Albarrán-Arriagada, F. Superconducting circuit architecture for digital-analog quantum computing. *EPJ Quantum Technol* **9**, 9 (2022).
41. Zhao, H., Wu, X., Li, W., Fang, X. & Li, T. Phase-Slip Based SQUID Used as a Photon Switch in Superconducting Quantum Computation Architectures. *Electronics (Basel)* **13**, 2380 (2024).
42. Wu, K., Bozzi, M. & Fonseca, N. J. G. Substrate Integrated Transmission Lines: Review and Applications. *IEEE Journal of Microwaves* **1**, 345–363 (2021).
43. Prostejovsky, A. M., Gehrke, O., Kosek, A. M., Strasser, T. & Bindner, H. W. Distribution Line Parameter Estimation Under Consideration of Measurement Tolerances. *IEEE Trans Industr Inform* **12**, 726–735 (2016).
44. Yun, K. Two types of electric field enhancements by infinitely many circular conductors arranged closely in two parallel lines. *Q Appl Math* **75**, 649–676 (2017).
45. Coufal, O., Radil, L. & Toman, P. Magnetic field and forces in a pair of parallel conductors. *International Journal of Applied Electromagnetics and Mechanics* **56**, 243–261 (2018).
46. Fedoseyev, V. G. Conservation laws and transverse motion of energy on reflection and transmission of electromagnetic waves. *J Phys A Math Gen* **21**, 2045–2059 (1988).
47. Kundu, S. & Simserides, C. Charge transport in a double-stranded DNA: Effects of helical symmetry and long-range hopping. *Phys Rev E* **109**, 014401 (2024).
48. Triberis, G. P., Simserides, C. & Karavolas, V. C. Small polaron hopping transport along DNA molecules. *Journal of Physics: Condensed Matter* **17**, 2681–2690 (2005).
49. Zhuravel, R. et al. Backbone charge transport in double-stranded DNA. *Nat Nanotechnol* **15**, 836–840 (2020).
50. Schilling, O. F. & Sugui, S. S. Faraday's law and perfect (super) conductivity. *Eur J Phys* **25**, 337–341 (2004).
51. Kühn, S. General Analytic Solution of the Telegrapher's Equations and the Resulting Consequences for Electrically Short Transmission Lines. *Journal of Electromagnetic Analysis and Applications* **12**, 71–87 (2020).
52. Reagor, M. J. Superconducting Cavities for Circuit Quantum Electrodynamics. (Yale University, Connecticut, 2015).
53. Frimmer, M. & Novotny, L. The classical Bloch equations. *Am J Phys* **82**, 947–954 (2014).
54. Stassi, R., Cirio, M. & Nori, F. Scalable quantum computer with superconducting circuits in the ultrastrong coupling regime. *npj Quantum Inf* **6**, 67 (2020).
55. Sabari, B. R., Dall'Agnese, A. & Young, R. A. Biomolecular Condensates in the Nucleus. *Trends Biochem Sci* **45**, 961–977 (2020).
56. Sharp, P. A., Chakraborty, A. K., Henninger, J. E. & Young, R. A. RNA in formation and regulation of transcriptional condensates. *RNA* **28**, 52–57 (2022).
57. Du, M. et al. Direct observation of a condensate effect on super-enhancer controlled gene bursting. *Cell* **187**, 331-344.e17 (2024).
58. Richter, W. F., Nayak, S., Iwasa, J. & Taatjes, D. J. The Mediator complex as a master regulator of transcription by RNA polymerase II. *Nat Rev Mol Cell Biol* **23**, 732–749 (2022).
59. Mann, R. & Notani, D. Transcription factor condensates and signaling driven transcription. *Nucleus* **14**, (2023).
60. Salari, H., Fourel, G. & Jost, D. Transcription regulates the spatio-temporal dynamics of genes through micro-compartmentalization. *Nat Commun* **15**, 5393 (2024).
61. Li, C., Li, Z., Wu, Z. & Lu, H. Phase separation in gene transcription control. *Acta Biochim Biophys Sin (Shanghai)* **55**, 1052–1063 (2023).

62. Cheng, Y., Zhang, Y. & McCammon, J. A. How Does the cAMP-Dependent Protein Kinase Catalyze the Phosphorylation Reaction: An ab Initio QM/MM Study. *J Am Chem Soc* **127**, 1553–1562 (2005).
63. Greiwe, J. F. et al. Structural mechanism for the selective phosphorylation of DNA-loaded MCM double hexamers by the Dbf4-dependent kinase. *Nat Struct Mol Biol* **29**, 10–20 (2022).
64. Weber, J. & Senior, A. E. ATP synthase: what we know about ATP hydrolysis and what we do not know about ATP synthesis. *Biochimica et Biophysica Acta (BBA) - Bioenergetics* **1458**, 300–309 (2000).
65. Kamerlin, S. C. L. & Warshel, A. On the Energetics of ATP Hydrolysis in Solution. *J Phys Chem B* **113**, 15692–15698 (2009).
66. Meurer, F., Do, H. T., Sadowski, G. & Held, C. Standard Gibbs energy of metabolic reactions: II. Glucose-6-phosphatase reaction and ATP hydrolysis. *Biophys Chem* **223**, 30–38 (2017).
67. Fagan, S. P. et al. Pyrophosphate release acts as a kinetic checkpoint during high-fidelity DNA replication by the *Staphylococcus aureus* replicative polymerase PolC. *Nucleic Acids Res* **49**, 8324–8338 (2021).
68. Da, L.-T. et al. A Jump-from-Cavity Pyrophosphate Ion Release Assisted by a Key Lysine Residue in T7 RNA Polymerase Transcription Elongation. *PLoS Comput Biol* **11**, e1004624 (2015).
69. Niepce, D., Burnett, J. J., Kudra, M., Cole, J. H. & Bylander, J. Stability of superconducting resonators: Motional narrowing and the role of Landau-Zener driving of two-level defects. *Sci Adv* **7**, (2021).
70. Boguslavski, K., Lappi, T., Peuron, J. & Singh, P. Conserved energy–momentum tensor for real-time lattice simulations. *The European Physical Journal C* **84**, 368 (2024).
71. Haroche, S. Cavity quantum electrodynamics: the strange properties of photons and atoms confined in a box. in *Quantum Electronics and Laser Science Conference 1992* (eds. E. Ippen, S. Chu, J. Shah & C. Weiman) vol. 13 (Anaheim, California United States, 1992).
72. Boyer, M., Liss, R. & Mor, T. Geometry of entanglement in the Bloch sphere. *Phys Rev A (Coll Park)* **95**, 032308 (2017).
73. McKay, D. C., Wood, C. J., Sheldon, S., Chow, J. M. & Gambetta, J. M. Efficient Z-Gates for Quantum Computing. *Phys Rev A (Coll Park)* **96**, 022330 (2017).
74. Bluvstein, D. et al. A quantum processor based on coherent transport of entangled atom arrays. *Nature* **604**, 451–456 (2022).
75. Hu, P., Li, Y., Mong, R. S. K. & Singh, C. Student Understanding of the Bloch Sphere. *Eur J Phys* (2024) doi:10.1088/1361-6404/ad2393.
76. Carbonell-Ballestero, M., Garcia-Ramallo, E., Montañez, R., Rodriguez-Caso, C. & Macía, J. Dealing with the genetic load in bacterial synthetic biology circuits: convergences with the Ohm's law. *Nucleic Acids Res* **44**, 496–507 (2016).
77. Petersson, K. D. et al. Circuit quantum electrodynamics with a spin qubit. *Nature* **490**, 380–383 (2012).
78. Hubač, I. Š. M. W. S. Quantum entanglement and quantum information in biological systems (DNA. in *Proceedings, Workshop on Black Holes and Neutron Stars (RAGtime 17-19)* (eds. Z. Stuchlík, G. Török & V. Karas) vol. 1 61–84 (2017).
79. Venta, R. et al. A processive phosphorylation circuit with multiple kinase inputs and mutually diversional routes controls G1/S decision. *Nat Commun* **11**, 1836 (2020).
80. Ye, B., Zheng, Z.-F. & Yang, C.-P. Multiplex-controlled phase gate with qubits distributed in a multicavity system. *Phys Rev A (Coll Park)* **97**, 062336 (2018).
81. Liu, T., Cao, X.-Z., Su, Q.-P., Xiong, S.-J. & Yang, C.-P. Multi-target-qubit unconventional geometric phase gate in a multi-cavity system. *Sci Rep* **6**, 21562 (2016).
82. Yang, C.-P., Chu, S.-I. & Han, S. Quantum Information Transfer and Entanglement with SQUID Qubits in Cavity QED: A Dark-State Scheme with Tolerance for Nonuniform Device Parameter. *Phys Rev Lett* **92**, 117902 (2004).